

AURORA: Adaptive Spreading Factor Control for Low-power Multihop LoRa Network

Eunjeong Park, Sungbo Eo, Hongchan Kim, Jeongyeup Paek, and Saewoong Bahk

Abstract—LoRa has gained significant attention for Internet of Things (IoT) applications that require low-power and long-range communication such as animal tracking. However, LoRa’s spreading factor (SF) selection mechanism and 1-hop topology lack effective per-link adaptation to dynamics of the communication channel nor provide comprehensive coverage of moving animals. To address this problem, we present *AURORA*, an adaptive and distributed SF control scheme for low-power multihop LoRa networks. *AURORA* exploits the key tradeoff of SF—receiver sensitivity vs. data rate—with a focus on energy efficiency. *AURORA* accurately predicts the packet delivery ratio (PDR) for each SF using efficient probing and model fitting techniques, enabling rapid per-link SF adaptation to improve both PDR and duty cycle in multihop networks. Through real-world experiments conducted on both indoor and outdoor testbeds, we demonstrate that *AURORA* effectively reduces energy consumption while ensuring reliable communication and extending network coverage. Compared to state-of-the-art approaches such as *ADR+*, *AURORA* improves the PDR by 14% and reduces the duty cycle by 18%.

Index Terms—IoT, LoRa, RPL, spreading factor, TSCH.

I. INTRODUCTION

ANIMAL tracking is a prominent Internet of Things (IoT) application that involves attaching communication-enabled sensor tags to animals for collecting location information and sensor data which is then transmitted to a server. It requires communication that is reliable, long-range, and energy-efficient, especially in the wild. An example of a commercial animal tracking system that we have tried using is the Druid’s Debut Nano sensor system [1] (Fig. 1). We attached sensor tags to the back of real turtles (Fig. 1(a)) to investigate the vegetation of invasive turtles for the purpose of eradicating them for the benefit of domestic ecosystem. However, this system is based on Bluetooth which has short

Manuscript received October 20, 2025; approved for publication November 4, 2025. This paper is specially handled by EIC and Division Editor with the help of three anonymous reviewers in a fast manner.

This research was supported by Institute of Information & communications Technology Planning & Evaluation (IITP) grant funded by the Korea government (MSIT) (No. IITP-2025-2021-0-02048 & IITP-2025-RS-2024-00405128), and also by the National Research Foundation of Korea (NRF) grant funded by the Korea government (MSIT) (No. RS-2024-00359450).

E. Park, S. Eo, H. Kim, and S. Bahk are with the Department of Electrical and Computer Engineering and INMC, Seoul National University, Seoul 08826, Republic of Korea, email: {ejpark, sbeo, hckim}@netlab.snu.ac.kr, sbahk@snu.ac.kr.

J. Paek is with the Department of Computer Science and Engineering, Chung-Ang University, Seoul 06974, Republic of Korea, email: jpaek@cau.ac.kr.

S. Bahk and J. Paek are the co-corresponding authors.

Digital Object Identifier: 10.23919/JCN.2025.000084

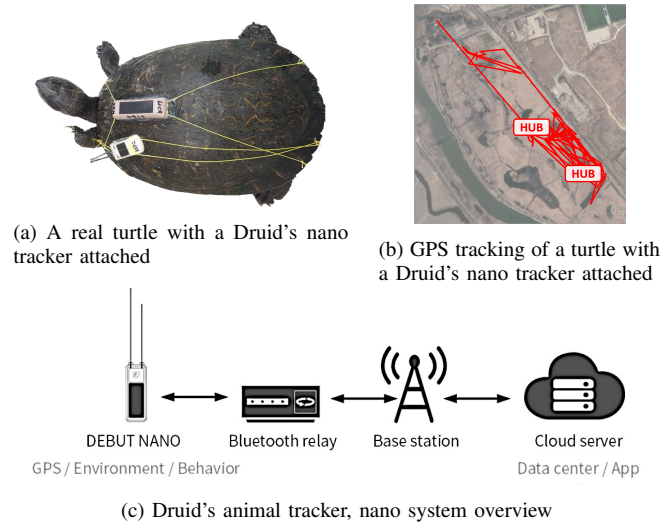


Fig. 1. An example animal tracking system (Druid) for investigating the vegetation of invasive turtles – a real deployment.

communication range and thus limited coverage, as exemplified in our collected data that had high density near the hub (gateway) but significantly less and intermittent data farther away (Fig. 1(b)).

LoRa has gained significant attention in IoT, particularly for applications that require extended communication ranges such as remote monitoring [2] and smart agriculture [3] where the network should cover a wide area but installing large number of gateways is not cost-effective. By capitalizing on sub-GHz channels and employing the *chirp spreading spectrum (CSS)* modulation, LoRa achieves coverage spanning kilometers with low energy consumption. On top of this long-range physical layer, LoRa’s link layer, recommended in the form of *LoRaWAN* by the LoRa Alliance [4], utilizes a star-topology centered around a powerful gateway that can manage multiple end devices.

LoRa’s 1-hop star-topology operation may suffice for many applications since it can typically cover up to a few kilometers. However, other applications such as animal tracking often require even broader coverage [5]–[7]. Covering several kilometers or more with LoRaWAN requires installation of multiple LoRa gateways in shadow areas as well as additional infrastructure such as back-bone networks and wired power. Consequently, expanding coverage for animal tracking, particularly at a low cost, is a challenging task.

An alternative that readily comes to mind for expanding coverage is to establish a multihop network, commonly

Creative Commons Attribution-NonCommercial (CC BY-NC).

This is an Open Access article distributed under the terms of Creative Commons Attribution Non-Commercial License (<http://creativecommons.org/licenses/by-nc/3.0>) which permits unrestricted non-commercial use, distribution, and reproduction in any medium, provided that the original work is properly cited.

adopted in low-power wireless sensor networks. Several prior work have already demonstrated the feasibility of LoRa multihop [8]–[10]. However, these studies overlook an important parameter of LoRa, the *Spreading Factor* (SF), which introduces a crucial and complex trade-off between receiver sensitivity, data rate, and energy efficiency in communication. While higher SF indeed enhances link reliability, its lower data rate and longer airtime can lead to increased collision probability and energy consumption.

A thread of research on LoRa have investigated the challenge of finding an appropriate SF parameter for 1-hop star topology [11]–[15]. However, these SF selection techniques rely on the legacy LoRaWAN with a powerful gateway, and does not support multihop. Adopting these techniques directly on non-gateway nodes for multihop proves challenging, as such nodes do not have the gateway’s multiple reception paths (circuits) and always-on capabilities.

To this end, we propose *AURORA*, an adaptive and distributed spreading factor control scheme for low-power multihop LoRa networks. *AURORA* extends the coverage of LoRa network using multihop over non-gateway nodes, while being reliable and energy-efficient using three key techniques: (1) adaptive per-link SF selection, (2) TSCH slot size adaptation for varying SF, and (3) RPL objective function design suitable for dynamic SF.

First, *AURORA* models the relationship between the SF and packet delivery ratio (PDR) for each link as a sigmoid function, and a convex-shaped prediction of energy consumption is obtained for each SF where the energy consumption is a function of data rate and PDR governed by SF. SF selection goes beyond simply settling for the current SF; it defines a probing probability to explore alternative SFs that may offer lower energy consumption or improved link stability.

Second, *AURORA* replaces the ALOHA-based MAC in LoRaWAN with the state-of-the-art *time-synchronized channel hopping* (TSCH) in IEEE 802.15.4 [16]. This is to address the LoRa’s vulnerability to packet collisions that worsens in multihop networks. However, adopting TSCH on LoRa is non-trivial because different SFs results in distinct packet airtimes, thus *requiring different timeslot sizes* and slot scheduling for each SF, and both the sender and receiver must align them for every transmission. *AURORA* is designed to adapt to these variations. An additional benefit of TSCH is that its synchronization mechanism facilitates SF negotiation between devices without additional overhead.

Finally, to enable multihop using non-gateway LoRa nodes, *IPv6 routing protocol for low-power and lossy network* (RPL) [17], [18] is adopted. However, distinct per-link SF affects reliability (PDR), airtime (data rate), and thus energy-efficiency (duty-cycle) of routing. Thus, we propose a new objective function that considers the SF of bi-directional links to and from a neighboring node when selecting routing parents. To the best of our knowledge, *AURORA* is the first multihop SF adaptation scheme that achieves energy-efficient and reliable LoRa coverage extension.

The contributions of this work are threefold.

- We model the key trade-offs of the spreading factor, and formulate an optimization problem for selecting the SF of

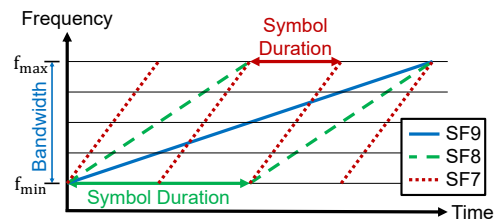


Fig. 2. The relationship between chirp duration and SF.

individual links in multihop LoRa, aimed at minimizing energy consumption while maximizing reliability.

- We propose *AURORA*, a LoRa protocol stack designed using the proposed LoRa SF optimization, TSCH slot adaptation, and RPL objective function design for dynamic SF.
- We implement *AURORA* on real embedded LoRa devices, and evaluate its performance extensively through indoor and outdoor experiments to demonstrate its effectiveness.

The paper is organized as follows: Section II provides the background of this work, and Section III present the design of the proposed *AURORA*. *AURORA* is evaluated in Section IV, and Section V concludes the paper.

II. BACKGROUND AND RELATED WORK

We begin by briefly introducing LoRa, TSCH, RPL, and their related prior work to motivate this work.

A. LoRa and Spreading Factor (SF)

LoRa is a low-power, long-range wireless communication protocol offering coverage up to several kilometers. This is made possible by its distinctive *CSS* modulation scheme, where a “chirp” represents a symbol whose carrier frequency changes at a fixed rate over time. This unique characteristic enables successful signal decoding even at much lower SNR compared to popular frequency-shift keying (FSK) modulation.

The main parameters that govern the shape and properties of a chirp are the *SF* and the bandwidth (*BW*). The symbol duration of a chirp (T_s) is set to $T_s = 2^{SF}/BW$. When the *BW* is fixed, the symbol rate decreases to half (equivalent to doubling the chirp duration) if *SF* increases by one (Fig. 2). The number of data bits per symbol (N_s) is equal to *SF*, and therefore the physical data rate can be calculated as,

$$\text{data rate} = N_s/T_s = SF \cdot BW/2^{SF}$$

Therefore, a higher *SF* and lower *BW* lead to a lower data rate. On the other hand, the chirp slope rate is determined as $BW/T_s = BW^2/2^{SF}$, and chirps with different slope rates (different *SF* given *BW* is fixed) are orthogonal to each other. This implies that chirps with different *SF* can be transmitted simultaneously without incurring collisions.

Given this relationship, LoRaWAN [4] incorporates a method called *adaptive data rate* (ADR) for selecting the SF of each node. The selection is based on the maximum SNR values of the last 20 packets compared with a predefined thresholds shown in Table I. ADR+ [19] improves this by considering

TABLE I
 SF-SPECIFIC SNR LIMITS FOR LoRA ADR.

SF	7	8	9	10	11	12
Relative air time	1	2	4	8	16	32
SNR limit (dB)	-7.5	-10	-12.5	-15	-17.5	-20

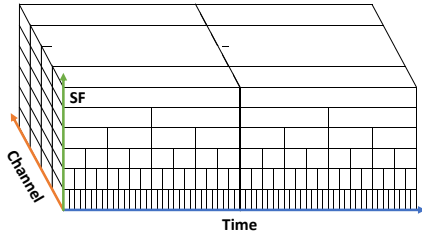


Fig. 3. An illustration of 3-dimensional TSCH cells composed of time offset, channel offset, and SF.

the average SNR of the last 20 packets. However, various studies [11], [20], [21] have criticized ADR for its failure to adequately adjust SF to link dynamics. In particular, the *ShuttleNet* [11] work addresses the need for SF selection reflecting mobility-induced link dynamics. The authors demonstrate that the ADR in LoRaWAN is insufficient, and propose a KNN algorithm-based SF adjustment to resolve this issue.

Other studies [12]–[15] have also proposed methods to adjust the SF of LoRa, but they are applicable only to 1-hop star-topology networks with high-cost gateways at the center. Gateways can simultaneously receive multiple packets with distinct SFs via parallel demodulation, but non-gateway nodes lack such capability. Since non-gateway LoRa nodes can listen to only one SF at a time, forming a multihop in LoRa requires a MAC protocol involving SF negotiation between a sender and a receiver. Moreover, since any node can potentially be a sender or a receiver in multihop topology, it is imperative for the SF selection process to be distributed, allowing each node to autonomously choose its transmission and reception SF without relying on a central coordinator. Furthermore, prior methods proposed for star-topology setups entail assumptions such as knowing the number and positions of all nodes, making them unrealistic for use in real multihop applications.

Another challenge of LoRa is that it is extremely vulnerable to collisions [22], [23]. A single star-topology network can mitigate this through gateway coordination, but collisions between multiple networks or distinct links within a multihop network cannot be eliminated by a gateway. There has been efforts to mitigate the problem in the physical (PHY) layer by enabling decoding of concurrent transmissions [24], [25]. Those approaches are orthogonal to our approach of resolving the problem in the medium access (MAC) layer, a natural place to handle multiple access of the channel, by adopting a well-established protocol as a basis.

B. TSCH

TSCH [16] is a time-synchronized channel-hopping MAC protocol defined in IEEE 802.15.4e that has demonstrated good performance in the literature for avoiding collisions [26]–[33].

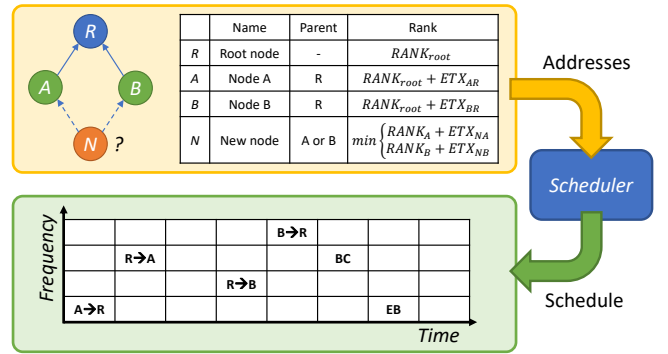


Fig. 4. RPL (top), TSCH (bottom), and the scheduler bridging the two (middle right).

TSCH divides time and frequency into timeslots and a channel set, where a *timeslot* is defined to be long enough to exchange a packet and an ACK given a fixed data rate (e.g., 10 ms for 250 kbps) [34]. A *cell* is the minimum unit of resource scheduling, defined as a timeslot and a channel represented by a time offset and a channel offset respectively:

$$t_{\text{offset}} = \text{ASN} \bmod L_{sf}, \quad (1)$$

$$\text{Channel} = \text{CHS}(\text{ASN} + c_{\text{offset}} \bmod L_{CHS}). \quad (2)$$

Absolute sequence number (ASN) denotes the timeslot's position from the beginning of the network, and slotframe length (L_{sf}) is the number of timeslots in a *slotframe*, the unit of repeated scheduling cycle. L_{CHS} is the length of the channel hopping sequence (CHS), and c_{offset} determines the actual channel to be used given the ASN and CHS. Nodes in the network periodically transmit enhanced beacons (EB) containing TSCH network information including ASN. A node seeking to join the network receives this EB and performs time synchronization to become part of the network.

A prior work on TSCH over LoRa [35] involves straightforward integration of existing TSCH implementation on LoRa devices. However, one oversight in this study is that as SF changes, the airtime varies even with a constant payload length, requiring different timeslot sizes. Therefore, another work [36] went further to define timeslot lengths differently for each SF, establishing the resource scheduling unit (cell) as a three-dimensional entity that incorporates time, channel, and SF as illustrated in Fig. 3. However, these studies do not propose methodologies for determining and exchanging appropriate SFs for each LoRa link within synchronized MACs, nor do they offer considerations for resource scheduling considering SFs.

C. RPL

RPL is an IPv6 routing protocol for low-power and lossy multihop wireless networks, tailored for resource-constrained IoT devices [17], [18]. RPL forms a tree-like topology towards a root node, where each non-root node selects a parent node that provides the shortest logical distance path leading to the root. The metric representing the logical distance between the root and a given node is denoted as the “rank.” A child node's rank is derived by adding the parent-child link metric (e.g.,

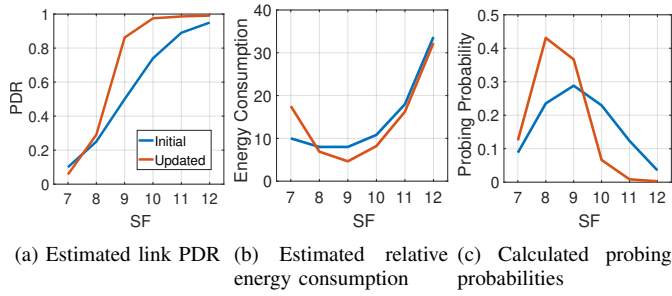


Fig. 5. Link PDR, relative energy consumption, and probing probability estimated or calculated in the initialization phase (blue line, initial SF of 9), and derived after exchanging packets (red line).

ETX) to the parent's rank, and the node selects the parent that minimizes its rank.

In prior work, efforts [8]–[10], [37], [38] have been made to construct LoRa multihop networks to extend coverage. However, these efforts have yet to address the challenge of selecting an appropriate SF for each link, nor have they elucidated how the chosen SF might impact the overall routing and network performance. Furthermore, these studies have been confined to small-scale experiments or have demonstrated performance through simulations only.

D. ALICE

TSCH standard defines time-slotted communication and channel hopping, but leaves *resource scheduling*—the selection of when (t_{offset}) and on which channel (c_{offset}) each device communicates—as an open problem. For example, a scheduler is necessary to allocate TSCH cells for transmission of RPL and data messages (Fig. 4). To fill this gap, various TSCH schedulers have been proposed [26]–[33], [39].

ALICE [27] is a state-of-the-art autonomous TSCH cell scheduler that relies only on ASN, sender address, and receiver address for scheduling without the need for separate information exchange:

$$H(A, B) = \text{Hash}(\alpha \cdot \text{ID}(A) + \text{ID}(B) + \text{ASN}), \quad (3)$$

$$t_{\text{offset}}(A, B) = H(A, B) \bmod L_{sf}, \quad (4)$$

where α represents the directionality between the sender and the receiver. Having the notion of link direction in the schedule, as in ALICE, is necessary to achieve SF consensus because the transmitter and receiver can only transmit and receive using a single SF at a time. Therefore, without loss of generality, we select ALICE as the TSCH scheduler for AURORA. However, we would like to emphasize that the problem we are solving is orthogonal to how the schedulers operate.

III. AURORA DESIGN

We present AURORA, a novel and holistic scheme that utilizes the characteristics of SF to enable reliable and energy efficient LoRa multihop. AURORA consists of three main parts: (1) adaptive selection of LoRa SF, (2) adopting TSCH on LoRa with varying slot sizes, and (3) re-designing RPL objective function for LoRa considering the key tradeoff of SF.

A. Adaptive SF Selection

We propose an SF selection algorithm to enhance LoRa's multihop performance. The proposed SF selection scheme consists of four steps: 1) initial SF selection and link PDR prediction, 2) energy consumption prediction and optimization, 3) probing probability determination, and 4) probing and data gathering. Then, steps 2) to 4) are repeated continuously.

Initial SF selection and PDR prediction. As SF increases, the PDR for a link approaches one, and as SF decreases, PDR approaches zero. This type of relationship is often modeled as a *sigmoid function*, and as such, we fit the PDR of each SF for a link to a sigmoid function.

$$\sigma(SF) = (1 + e^{-SF})^{-1}, \quad SF = 7 : 12. \quad (5)$$

However, since there is no channel information during the initialization period, AURORA starts with an initial SF chosen according to the SNR values of the first few received broadcast packets (i.e., TSCH EB or RPL DIO) and a mapping table between SF and their minimum required SNR (Table I) in a similar way as ADR in LoRaWAN. In ADR, the SNR-SF mapping is derived from BER of 0.001. This corresponds to a PDR of 0.5 assuming a packet size of approximately 87 bytes [40], which is the median value of the sigmoid function. From this observation, we select the initial SF (SF_{init}) according to SNR, and use it as the center of the sigmoid (SF_m) as follows;

$$PDR(SF) = (1 + e^{-\omega(SF - SF_m)})^{-1}, \quad (6)$$

$$SF_m = SF_{\text{init}} = f_{\text{ADR}}(\text{SNR}_{\text{init}}). \quad (7)$$

Here, ω can be regarded as the slope of the sigmoid function. The resulting initial model for the estimated PDR will be continuously updated at runtime as packet exchanges occur, as shown in Fig. 5(a).

Energy consumption prediction. The advantage of fitting the PDR of SF to a sigmoid function is that ETX can be expressed simply as below;

$$ETX(SF) = PDR(SF)^{-1} = 1 + e^{-\omega(SF - SF_m)}. \quad (8)$$

Then, the trend that ETX approaches one as SF increases is also consistent with reality. We can obtain the relative energy consumption E_{rel} as the *expected total air time* of a packet by multiplying ETX with the *relative air time* T_{rel} because ETX is the number of transmissions required to send one packet successfully and the energy required for one transmission is proportional to T_{rel} given that the peak power does not vary according to SF [41].

$$T_{\text{rel}}(SF) = 2^{SF}, \quad (9)$$

$$E_{\text{rel}}(SF) = ETX \cdot T_{\text{rel}} = (1 + e^{-\omega(SF - SF_m)}) \cdot 2^{SF}. \quad (10)$$

Since ETX and T_{rel} are both exponential convex functions, E_{rel} also becomes a convex function which has a minima as shown in Fig. 5(b).

Probing probability. During the initialization step, the initial SF and corresponding PDR are estimated. However, since this estimate may differ from the actual at run-time, AURORA occasionally probes the channel with other SFs. This is done

during normal data transmissions and does not require sending additional probing packets. Furthermore, it is unnecessary to probe all other SFs with equal probability. *AURORA* probes SFs with low energy consumption more often, and SFs with higher energy consumption less frequently. Specifically, we differentiate the PDR function and normalize it to obtain the probing probability $PDF(SF)$. The blue line in Fig. 5(c) depicts this probing probability during the initialization phase.

$$PDF(SF) = c \cdot PDR'(SF). \quad (11)$$

The SF that minimizes energy is found within ± 0.5 of the inflection point on the PDR sigmoid graph. This is proved as follows: Since the PDR is represented by a sigmoid function and energy consumption is represented in the form of $2^x/PDR$, we simplify PDR and relative air-time to $f(x) = \sigma(b(x-a))$ and $g(x) = 2^x$, respectively. The inflection point of PDR occurs where the second derivative of $f(x)$ is zero.

$$f(x) = \sigma(b(x-a)), \quad (12)$$

$$f''(x) = b^2 f(x)(1-f(x))(1-2f(x)) = 0, \quad (13)$$

$$\therefore x = a. \quad (14)$$

On the other hand, the point where energy consumption is minimized is the point where the first derivative of $g(x)/f(x)$ equals 0. Differentiating this, we get the following:

$$\left(\frac{g(x)}{f(x)} \right)' \Big|_{x=a+\frac{1}{b} \ln\left(\frac{b-\ln(2)}{\ln(2)}\right)} = 0. \quad (15)$$

Here, the value of $\frac{1}{b} \ln\left(\frac{b-\ln(2)}{\ln(2)}\right)$ falls within ± 0.5 for b values of 1.1 and above.

This indicates that the SF which minimizes energy consumption lies within ± 0.5 of the inflection point of the PDR curve, making it energy-efficient to concentrate probing efforts around this region. This approach also enhances the efficiency of PDR prediction by leveraging the characteristics of the sigmoid function. In a sigmoid function, the rate of change in the output (y) diminishes as the input (x) moves further from the inflection point. As a result, PDR data far from the inflection point contribute little to accurately estimating the function parameters. Therefore, *AURORA* gathers more meaningful channel information by selectively probing alternate SFs near the one estimated to yield the lowest energy consumption.

Probing and data gathering. Now that *AURORA* has determined the initial SF and the probing probability for selecting an alternative SF, it proceeds with communication based on the defined probing strategy. Since the PDRs for each SF were collected through transmissions that also functioned as probing, it becomes possible to refine key parameters for more accurate PDR prediction across different SFs. The proposed scheme identifies a set of parameters—specifically, the slope and center of the sigmoid function—that minimizes the L2 norm between the generated PDR curve and the measured PDR values. This optimization enables updates to the predicted PDR, which in turn allows for recalculation of both the energy consumption model and the probing probability.

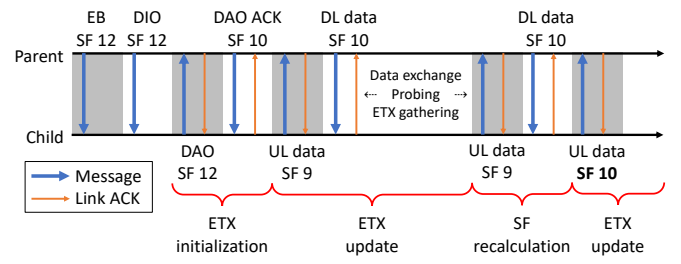


Fig. 6. The SF negotiation and update procedure. Nodes initially receive EB and DIO messages, followed by mutual SF initialization through DAO and DAO ACK messages. Subsequently, nodes update ETX via unicast packet exchanges, resulting in the selection of a more energy-efficient SF.

The red lines in Fig. 5 illustrate the calculated PDR, energy consumption, and probing probability after applying the SF selection algorithm based on real measurement data. At this stage, the sigmoid function and its deviation are particularly advantageous, as they require only simple exponential operations. To support deployment on resource-constrained nodes, exponential values are precomputed and stored, enabling efficient computation with minimal processing overhead.

B. Applying TSCH & RPL to LoRa Network

Considering LoRa's SF, the process of using TSCH and RPL together is accompanied by three mechanisms besides the operations mentioned in Section II: SF negotiation, time offset re-location, and RPL rank calculation considering SF.

SF negotiation. First of all, for essential broadcast messages such as TSCH EB, RPL DIO, and RPL DAO, we use a fixed SF of 12 to make a conservative effort to form a stable and reliable network. The actual performance gain in *AURORA* stems from unicast data transmissions enabled by optimal SF selection. To support this, *AURORA* embeds its SF selection mechanism within unicast transmissions, leveraging link-layer ACKs to compute both the PDR and ETX. When a node first detects a neighbor, it initializes the PDR values for SFs 7 to 12 as outlined in Section III-A. During subsequent data exchanges, the node updates PDR values based on transmission success or failure. Since SFs are chosen probabilistically for probing, this naturally results in a diverse set of link quality measurements. After a predefined number of successful transmissions (e.g., 10), the SF fitting process is initiated. The node then finalizes SF selection through a negotiation step using link-layer ACKs, as depicted in Fig. 6.

Fitting the PDR with a sigmoid function proves beneficial in terms of ACK overhead reduction. This is because the sigmoid function can be expressed solely by ω and SF_m . Consequently, while the original probing required at least 6 bytes for transmission, the sigmoid fitting approach enables transmitting the same information with only 2 bytes. As a result, the ACK overhead for SF negotiation is also reduced.

Time offset re-location. Prior research [36] suggests that different cell lengths should be used for each SF in a network where time is divided into cells of a specific length. Here, we further explain how to set SF offset and the time offset when using TSCH, with the ALICE scheduler as an example.

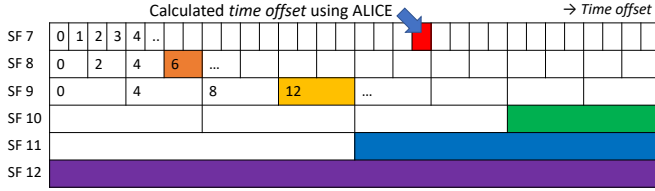


Fig. 7. Adaptation of time offset according to SF. This example illustrates when the time offset for SF 7 is 19, and $L_{sf,UC}$ is 32.

The primary reason for choosing ALICE over other schedulers is its directional characteristic. Other receiver-based or sender-based schemes are not suitable for managing various SFs. For instance, in a receiver-based scheduler, a node wakes up once per schedule to listen. If other nodes wanting to transmit to this node use different SFs, the receiving node cannot determine which SF to receive on. Similarly, in a sender-based scheme, the sender does not know the receiver's SF, so it is unsure which SF to use for sending. Consequently, it might need to try all SFs, or the entire network might need to use a single SF. ALICE addresses this by using the sender's address and ASN in a hash function to schedule cells according to the link direction between parent and child.

If the aforementioned probing approach in Section III-A is purely probabilistic, the sender and receiver will not be able to rendezvous on the same SF. Therefore, in *AURORA*, pseudo-random numbers are generated through a hash function and used to select an SF to be probed:

$$x_{SF}(A, B) = (H(A, B) \bmod 100) / 100, \quad (16)$$

$$\begin{aligned} SF(A, B) &= \lfloor CDF^{-1}(x_{SF}(A, B)) \rfloor, \\ &= \lfloor PDR^{-1}(x_{SF}(A, B)) \rfloor. \end{aligned} \quad (17)$$

The input to the hash function includes the ASN and the link-layer addresses of both the sender and receiver, allowing them to derive the same value within a given cell. If the resulting hash value is less than the cumulative value of the probing function, the corresponding SF is selected for use.

Since we aim to adapt TSCH timeslot lengths based on the selected SF, the time offset must also be readjusted accordingly. As the SF increases by one, the airtime doubles. To accommodate this, we double the cell's timeslot length for each one-step increase in SF. The time offset for SF 7 is determined using (4). This offset is multiplied by the relative airtime of the selected SF, and the result is taken modulo the unicast slotframe length to obtain the new time offset. For example, when the time offset calculated by ALICE corresponds to the position indicated by the arrow in Fig. 7, the timeslot length for SFs 7 through 12 increases sequentially, doubling at each step. As a result, the time offset is readjusted to align with the start of the overlapping cell, which can be computed using the following formula:

$$t_{\text{offset},7} = H(A, B) \bmod L_{sf,UC}, \quad (18)$$

$$t_{\text{offset},SF} = t_{\text{offset},7} \times 2^{SF-7} \bmod L_{sf,UC}. \quad (19)$$

Rank re-calculation. Adjusting the SF directly affects the ETX, while the rank in RPL is computed based on accumulated ETX. Thus, rank calculation must take SF into account.

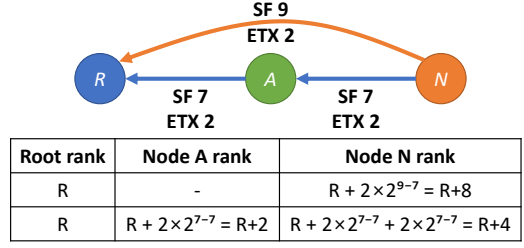


Fig. 8. An example of applying the new objective function. The first row represents the legacy scenario where traffic bypasses parent A, while the second row illustrates the proposed approach where traffic traverses through A using a lower SF for transmission.

For this purpose, *AURORA* introduces a new RPL objective function named *expected air time objective function* (EAT-OF), which explicitly accounts for dynamic SF to minimize overall network energy consumption. The intuition behind EAT-OF is illustrated in Fig. 8. Since airtime doubles with each increment in SF, transmitting a given distance in two hops using SF 7 may consume less energy than transmitting it in a single hop using SF 9. Even though the transmission involves an additional intermediate node, this results in an overall energy gain for the network.

In EAT-OF, the relative air time (T_{rel}) of the currently used SF is multiplied to ETX before adding it to the rank. The physical meaning of adding $ETX \cdot T_{rel}$ to the parent's rank is to add the amount of energy required to successfully send a packet to the parent, given SF 7 with PDR 100% as the baseline. Then, selecting a parent candidate that has the lowest rank means finding the least-energy cost path to the root.

However, since unicast communication with ACK exchange occurs only between the selected parent and child, it is difficult to determine the most appropriate SF for other potential parent candidates, as their ETX information is not available. The only information available for a parent candidate comes from the multicast DIO messages it transmits. This includes DAG-related information, the node's address, its rank, and the received signal strength of the DIO itself. Thus, EAT-OF estimates the appropriate SF and corresponding ETX for a parent candidate by comparing the SNR of its DIO message with that of the currently selected preferred parent. Specifically, following a strategy similar to LoRaWAN's ADR mechanism, the SF is adjusted by one step for every 2.5 dB difference in received SNR.

$$SF_{new} = SF_{prefer} + (SNR_{prefer} - SNR_{new}) / 2.5. \quad (20)$$

For example, let's assume that node A is currently the preferred parent that can communicate with SF 9, and the SNR of multicast DIO received from it is -16 dB. When the SNR of DIO received from node B is -11 dB, it is assumed that SF 7 is suitable for node B. Also, when the SNR of DIO received from node C, another parent candidate, is -21 dB, it assumes that SF 11 is suitable for communication with node C. Through this EAT-OF, *AURORA* can calculate the expected rank of every parent candidate, and construct an energy efficient routing topology.

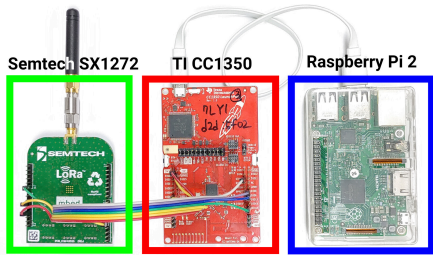


Fig. 9. Each node in the experimental setup is equipped with a Semtech SX1272 LoRa communication module, a TI CC1350 MCU, and a Raspberry Pi 2 for logging purposes.

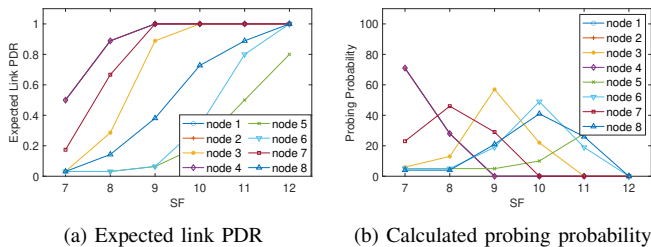


Fig. 10. Expected PDR and calculated probing probability, after applying the SF selection to a 1-hop network with 8 nodes.

IV. EVALUATION

We implement *AURORA* on real embedded devices to evaluate its performance, and compare it against ADR+ and fixed SF configurations on 9- and 12-node testbeds.

A. Experiment Setup

For the hardware, Semtech SX1272 and TI CC1350 are used in each node for the LoRa module and the MCU respectively, as shown in Fig. 9. For the software, we use TSCH-over-LoRa [35] code in Contiki-NG OS as the basis, and implement *AURORA* by modifying the operations of TSCH, ALICE, and RPL. For comparison, we implement ADR+ [19] which selects SF based on the average SNR of the last 20 packets.

In the experiments, 4 channels are used, and the timeslot length for SF 7 is set to 0.3125 seconds (i.e., 10sec for SF 12), with an EB period of 5 minutes and a DIO period of 30 minutes. A slotframe consists of thirty-one SF 12 slots for EB, eleven SF 12 slots for shared slots (i.e., for RPL DIO and DAO), and seven SF 12 slots for unicast transmissions. The transmit power is set to 14 dBm, and an attenuator of 30 dB is used for reducing the signal strength to mimic large scale deployments.

The experiments are conducted within a laboratory building, with a total of 9 nodes (1 root node and 8 non-root nodes) for 1-hop experiments on floors 3 and 4, and 12 nodes (1 root node and 11 non-root nodes) for multihop experiments on floors 1 to 3. The data transmission period is set to 10 minutes for 1-hop experiments and 20 minutes for multihop experiments.

B. Adaptive SF Selection and Scheduling

We first evaluate the performance of the proposed adaptive SF selection scheme against fixed SF 7-to-12 and ADR+. To

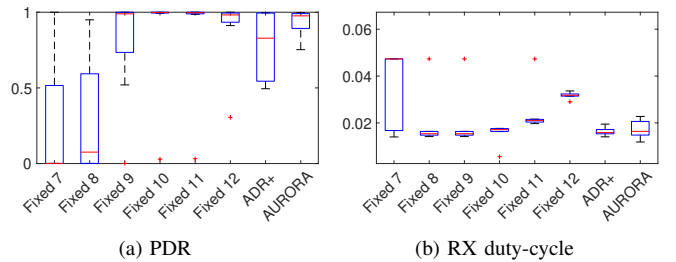


Fig. 11. Performance comparison of fixed SF schemes, ADR, and the proposed *AURORA* in a 1-hop testbed.

TABLE II
MOST FREQUENTLY SELECTED SFs FOR EACH NODE AND THEIR AVERAGE SNR.

Node	1	2	3	4	5	6	7	8
Avg. SNR (dB)	-3.3	-1.7	-8.9	-4.5	-11.7	-10.8	-7.4	-14.1
ADR+ SF	8	7	9	7	9	7	7	10
AURORA SF	7	7	8	7	11	10	8	10
SF difference	-1	0	-1	0	+2	+3	+1	0

compare the SF selection techniques while minimizing the effect of other variables, we enforce a 1-hop topology on 8 non-root nodes using DIO blacklisting (i.e., discard DIOs from other non-root nodes). The SFs selected by *AURORA* and ADR+ are outlined in Table II, and their expected link PDR and probing probability are shown in Figs. 10(a) and 10(b). Although the selected SFs did not differ significantly, the minor differences had a notable impact: higher SFs increased energy consumption, while lower SFs resulted in lower PDR.

Fig. 11(a) plots the actual measured end-to-end PDR results where *AURORA* demonstrates an average PDR of 99%, significantly higher than ADR+, while having similar duty-cycle in Fig. 11(b). Although a certain fixed SF can either achieve a better PDR or lower duty-cycle in some cases, but not both at the same time. Furthermore, optimal fixed SF for each link cannot be known a priori and will not work under dynamic channel conditions. In contrast, *AURORA* selects SFs to ensure high PDR with low duty cycle, and adapts it to channel dynamics at run-time (Fig. 13).

Next, we validate whether the SF negotiation and time offset reallocation within TSCH and ALICE are operating as intended. Fig. 12 depicts the schedules of eight nodes over four SF 12 cells, excluding channel offsets for visibility. It demonstrates that the time offset varies effectively according to the selected SFs as proposed in Section III. As an example, Fig. 13 illustrates the SFs selected by a node (node 5) over packet numbers. Despite changes in SF over time, the negotiation between the root and the node ensures that the connection remains stable and transmission slots are scheduled correctly with varying slot sizes considering the SF adaptation.

C. Multihop Experiment

We next construct a 12-node multihop network using *AURORA*. These experiments took place in floors 1 to 3 of a university building, with 4 nodes installed on each floor. While other low-power radios such as the IEEE 802.15.4 in 2.4 GHz would have had difficulty in constructing a network

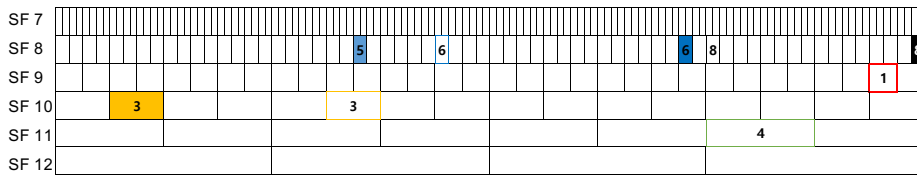


Fig. 12. Root's cell scheduling result of 8 non-root nodes within four SF 12 cells. The numbers indicate the node ID, and the filled boxes represent RX slots, while unfilled boxes denote TX slots.

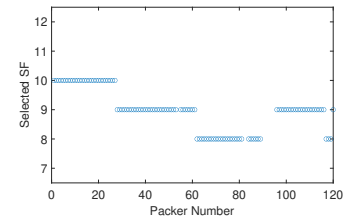
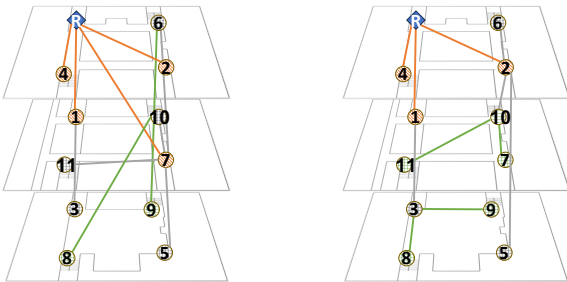


Fig. 13. SF variation of node 5 according to the packet number.



(a) Multihop topology w/o EAT-OF (b) Multihop topology with EAT-OF

Fig. 14. Topology comparison with and without EAT-OF.

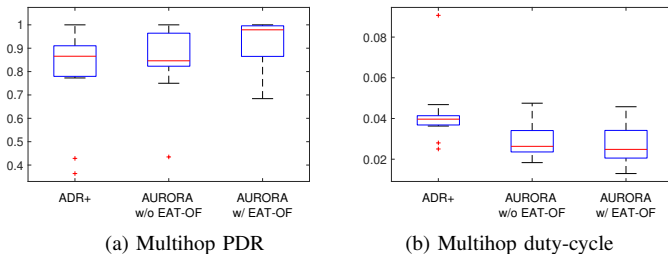


Fig. 15. Performance comparison of ADR+ and *AURORA* with and without modifying the RPL objective function.

in such a setup due to distances and obstacles, LoRa's ability to decode signals under very low SNR necessitates the use of attenuators to create a LoRa multihop network within the building setting. The resulting RPL tree topology is depicted in Fig. 14, with and without EAT-OF¹. EAT-OF incorporates SF into the rank calculation by predicting SF based on the preferred parent and the SNR difference, leading to changes in topology. In particular, node 7 and node 11 found more energy-efficient paths, moving from 1-hop and 2-hop positions to 3-hop positions, respectively. Experiment results in Fig. 15 demonstrate that by considering the SF and the rank of the new parent, *AURORA* improves the PDR by 14% and reduces the duty cycle by 18%.

D. Long-distance Outdoor Experiment

All experiments so far have been conducted in controlled indoor environments. However, to achieve the primary objective of this study which is to extend LoRa coverage for animal tracking, it is imperative to demonstrate the system's efficacy in outdoor environment. In this subsection, we assess the performance of *AURORA* in a large-scale outdoor environment

¹For 'without EAT-OF', we use the default MRHOF with ETX in RPL

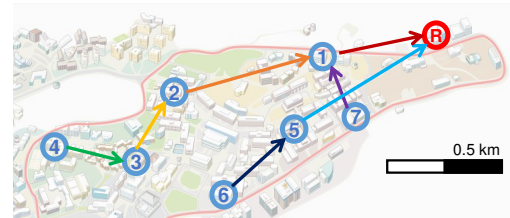


Fig. 16. Map of the experiment site and the multihop topology. Experiments are conducted within a campus area of $\sim 3.90 \text{ km}^2$, with a maximum straight-line distance of 1.61 km between nodes.

TABLE III
SF AND PDR ACHIEVED IN THE OUTDOOR EXPERIMENT.

Node number	1	2	3	4	5	6	7
Most selected SF	9	11	11	12	11	12	11
PDR (%)	99	90	92	63	98	92	98

with obstructions. We deploy one root node and seven non-root nodes on the rooftops of buildings across a campus with an area of approximately 3.90 km^2 , as illustrated in Fig. 16. While the root node maintained line-of-sight (LoS) with all non-root nodes, the non-root nodes were in non-line-of-sight (NLoS) relative to each other. Each node is configured to join the *AURORA* network and transmit data packets every 10 minutes. The equipment used in this experiment is the same as in previous experiments, but with the attenuators removed and replaced with 3 dBi antennas. Considering the dynamic outdoor environment, the initial SF is conservatively adjusted to 12 to accommodate potential variability.

The 24-hour experiment resulted in a network topology of up to four hops as shown in Fig. 16. The selected SF and PDR are presented in Table III. A significant number of data packets were relayed through a non-root node 1, which was deemed a good path by *AURORA* since it was able to use a relatively low SF due to its direct LoS connection to the root node. However, other nodes, being in NLoS conditions with each other had relatively higher SF, and thus were less selected as routing paths. This experiment demonstrates that *AURORA* is viable for use in outdoor environments, thereby validating its applicability for real-world animal tracking scenarios.

V. CONCLUSION

We proposed *AURORA*, an adaptive and distributed spreading factor control scheme for low-power multihop LoRa networks. *AURORA* leverages the key tradeoff of SF with a specific focus on energy efficiency. By accurately predicting

the packet delivery ratio for each SF through efficient probing and model fitting techniques, *AURORA* enables rapid per-link SF adaptation, improving PDR and reducing duty-cycle over multihop networks. We also integrated the advanced TSCH MAC and RPL routing protocols to LoRa with careful re-design of timeslot and objective function for more reliable and energy-efficient operation with dynamic SF. To the best of our knowledge, this is the first multihop SF adaptation scheme. Experiments on real testbeds demonstrate that *AURORA* effectively reduces duty-cycle by 18% and improves packet delivery ratio by 14% compared to ADR+ while extending network coverage.

REFERENCES

- [1] D. Technology, "DEBUT NANO." 2024. [Online]. Available: <https://druid.tech/products/debut-series/debut-nano/>
- [2] J. P. Shanmuga Sundaram, W. Du, and Z. Zhao, "A survey on LoRa networking: Research problems, current solutions, and open issues," *IEEE Commun. Surveys Tuts.*, vol. 22, no. 1, pp. 371–388, 2020.
- [3] A. Pagano, D. Croce, I. Tinnirello, and G. Vitale, "A survey on LoRa for smart agriculture: Current trends and future perspectives," *IEEE Internet Things J.*, vol. 10, no. 4, pp. 3664–3679, 2023.
- [4] LoRa Alliance, "What is LoRaWAN® specification," 2019. [Online]. Available: <https://loro-alliance.org/about-lorawan/>
- [5] B. S. Chaudhari, M. Zennaro, and S. Borkar, "LPWAN technologies: Emerging application characteristics, requirements, and design considerations," *Future Internet*, vol. 12, no. 3, 2020.
- [6] U. Raza, P. Kulkarni, and M. Sooriyabandara, "Low power wide area networks: An overview," *IEEE Commun. Surveys Tuts.*, vol. 19, no. 2, pp. 855–873, 2017.
- [7] G. A. Akpakwu, B. J. Silva, G. P. Hancke, and A. M. Abu-Mahfouz, "A survey on 5G networks for the Internet of Things: Communication technologies and challenges," *IEEE Access*, vol. 6, pp. 3619–3647, 2018.
- [8] B. Sartori, S. Thielemans, M. Bezunarte, A. Braeken, and K. Steenhaut, "Enabling RPL multihop communications based on LoRa," in *Proc. IEEE WiMob*, 2017.
- [9] C.-H. Liao, G. Zhu, D. Kuwabara, M. Suzuki, and H. Morikawa, "Multi-Hop LoRa networks enabled by concurrent transmission," *IEEE Access*, vol. 5, pp. 21430–21446, 2017.
- [10] P. Tian, C. A. Boano, X. Ma, and J. Wei, "LoRaHop: Multihop support for LoRaWAN uplink and downlink messaging," *IEEE Internet Things J.*, vol. 10, no. 17, pp. 15376–15392, 2023.
- [11] D. Mu, Y. Chen, J. Shi, and M. Sha, "Runtime control of LoRa spreading factor for campus shuttle monitoring," in *Proc. IEEE ICNP*, 2020.
- [12] W. Gao, Z. Zhao, and G. Min, "AdapLoRa: Resource adaptation for maximizing network lifetime in LoRa networks," in *Proc. IEEE ICNP*, 2020.
- [13] E. F. Silva *et al.*, "Adaptive parameters for LoRa-based networks physical-layer," *Sensors*, vol. 23, no. 10, 2023.
- [14] A. Loubany, S. Lahoud, and R. El Chall, "Adaptive algorithm for spreading factor selection in LoRaWAN networks with multiple gateways," *Comput. Netw.*, vol. 182, p. 107491, 2020.
- [15] M. Bor and U. Roedig, "LoRa transmission parameter selection," in *Proc. DCOSS*, 2017.
- [16] "IEEE Standard for local and metropolitan area networks—Part 15.4: Low-Rate wireless personal area networks (LR-WPANs) amendment 1: MAC sublayer," IEEE, Standard, 2012.
- [17] R. Alexander *et al.*, "RPL: IPv6 routing protocol for low-power and lossy networks," RFC 6550, 2012.
- [18] H.-S. Kim, J. Ko, D. E. Culler, and J. Paek, "Challenging the IPv6 routing protocol for low-power and lossy networks (RPL): A survey," *IEEE Commun. Surveys Tuts.*, vol. 19, no. 4, pp. 2502–2525, 2017.
- [19] M. Slabicki, G. Prensankar, and M. Di Francesco, "Adaptive configuration of LoRa networks for dense IoT deployments," in *Proc. IEEE/IFIP NOMS*, 2018.
- [20] N. Benkahla, H. Tounsi, Y.-Q. Song, and M. Frikha, "Enhanced ADR for LoRaWAN networks with mobility," in *Proc. IWCMC*, 2019.
- [21] F. Cuomo *et al.*, "EXPLoRa: Extending the performance of LoRa by suitable spreading factor allocations," in *Proc. IEEE WiMob*, 2017.
- [22] A. Rahmadhani and F. Kuipers, "When LoRaWAN frames collide," in *Proc. ACM WiNTECH*, 2018.
- [23] S. Tong, J. Wang, and Y. Liu, "Combating packet collisions using non-stationary signal scaling in LPWANs," *IEEE/ACM Trans. Netw.*, vol. 30, no. 3, pp. 1104–1117, 2022.
- [24] G. Lee, E. Park, M. Park, J. Paek, and S. Bahk, "BIC-LoRa: Bits in chirp shapes to boost throughput in LoRa," in *Proc. ACM/IEEE IPSN*, 2024.
- [25] M. O. Shahid, M. Philipose, K. Chintalapudi, S. Banerjee, and B. Krishnaswamy, "Concurrent interference cancellation: Decoding multi-packet collisions in LoRa," in *Proc. ACM SIGCOMM*, 2021.
- [26] S. Duquenooy, B. Al Nahas, O. Landsiedel, and T. Watteyne, "Orchestra: Robust mesh networks through autonomously scheduled TSCH," in *Proc. ACM SenSys*, 2015.
- [27] S. Kim, H.-S. Kim, and C. Kim, "ALICE: Autonomous link-based cell scheduling for TSCH," in *Proc. ACM/IEEE IPSN*, 2019.
- [28] S. Jeong, H.-S. Kim, J. Paek, and S. Bahk, "OST: On-demand TSCH scheduling with traffic-awareness," in *Proc. IEEE INFOCOM*, 2020.
- [29] S. Kim, H.-S. Kim, and C.-k. Kim, "A3: Adaptive autonomous allocation of TSCH slots," in *Proc. ACM/IEEE IPSN*, 2021.
- [30] Z. Yu *et al.*, "SmarTiSCH: An interference-aware engine for IEEE 802.15.4e-based networks," in *Proc. ACM/IEEE IPSN*, 2022.
- [31] S. Jeong, J. Paek, H.-S. Kim, and S. Bahk, "TESLA: Traffic-aware elastic slotframe adjustment in TSCH networks," *IEEE Access*, vol. 7, pp. 130468–130483, 2019.
- [32] J. Jung, D. Kim, T. Lee, J. Kang, N. Ahn, and Y. Yi, "Distributed slot scheduling for QoS guarantee over TSCH-based IoT networks via adaptive parameterization," in *Proc. ACM/IEEE IPSN*, 2020.
- [33] J. Shin, H. Kim, J. Paek, and S. Bahk, "ECA: Exclusive cell allocation for autonomous scheduling in time-slotted channel hopping," in *Proc. IEEE MASS*, 2023.
- [34] H. Kim, G. Lee, J. Shin, J. Paek, and S. Bahk, "Slot-size adaptation and utility-based packet aggregation for IEEE 802.15.4e time-slotted communication networks," *IEEE Internet Things J.*, vol. 11, no. 9, pp. 16382–16397, 2024.
- [35] M. Haubro, C. Orfanidis, G. Oikonomou, and X. Fafoutis, "TSCH-over-LoRa: Long range and reliable IPv6 multi-hop networks for the Internet of Things," *Internet Technol. Lett.*, vol. 3, no. 4, p. e165, 2020.
- [36] H. Soy, "An adaptive spreading factor allocation scheme for mobile LoRa networks: Blind ADR with distributed TDMA scheduling," *Simulation Modelling Practice Theory*, vol. 125, p. 102755, 2023.
- [37] A. Scarvaglieri, A. Panebianco, and F. Busacca, "MAGELLAN: A distributed MAB-based algorithm for energy-fair and reliable routing in multi-hop LoRa networks," in *Proc. IEEE GLOBECOM*, 2024.
- [38] G. Leenders *et al.*, "An energy-efficient LoRa multi-hop protocol through preamble sampling for remote sensing," *Sensors*, vol. 23, no. 11, 2023. [Online]. Available: <https://www.mdpi.com/1424-8220/23/11/4994>
- [39] H. Kim, G. Lee, J. Shin, J. Paek, and S. Bahk, "Quick6TiSCH: Accelerating formation of 6TiSCH networks with TSCH and RPL," in *Proc. IEEE MASS*, 2024.
- [40] L. Casals, C. Gomez, and R. Vidal, "Understanding the impact of packet size on the energy efficiency of LoRaWAN," *J. Commun. Netw.*, vol. 25, no. 6, pp. 814–824, 2023.
- [41] L. Casals, B. Mir, R. Vidal, and C. Gomez, "Modeling the energy performance of LoRaWAN," *Sensors*, vol. 17, no. 10, 2017.



Eunjeong Park received her B.S. degree in Electrical and Computer Engineering from Seoul National University (SNU), Seoul, Republic of Korea, in 2016, and her Ph.D. degree from the same university in August 2024. She is currently with Samsung Research, Seoul, Republic of Korea, where she has been working since September 2024. Her research interests include sensor networks, Bluetooth Low Energy, and wireless IoT system.



Sungbo Eo received the B.S. degree in Electrical and Computer Engineering from Seoul National University, Seoul, Republic of Korea, in 2021, where he is currently pursuing the Ph.D. degree. His research interests include Internet of Things and protocol design in wireless networks.



Hongchan Kim received the B.S. and Ph.D. degrees in Electrical and Computer Engineering from Seoul National University (SNU), Seoul, Republic of Korea, in 2015 and 2023, respectively. From August 2023 to August 2025, he was with LG Electronics, Seoul, where he worked on 3GPP RAN2 standardization, focusing on Ambient IoT and control plane protocol design. Since September 2025, he has been a Postdoctoral Researcher with the Institute of New Media and Communications (INMC) and the Ubiquitous Network Laboratory (NETLAB), SNU.

His research interests include wireless IoT systems, 5G/6G networks, and the integration of AI and networking.



Jeongyeup Paek is a Tenured Professor and the Department Chair at the Department of Computer Science and Engineering, Chung-Ang University, Seoul, Republic of Korea. He received his B.S. degree from Seoul National University in 2003 and his M.S. degree from University of Southern California (USC) in 2005, both in Electrical Engineering. He then received his Ph.D. degree in Computer Science from USC in 2010. He worked at Deutsche Telekom R&D Labs USA as a research intern in 2010, and then joined Cisco Systems in 2011 where he was a

Technical Leader in the Internet of Things Group. In 2014, he was with the Hongik University, Department of Computer Information Communication as an Assistant Professor.



Saewoong Bahk received the B.S. and M.S. degrees in Electrical Engineering from Seoul National University (SNU), in 1984 and 1986, respectively, and the Ph.D. degree from the University of Pennsylvania, in 1991. He was with AT&T Bell Laboratories as a Member of Technical Staff, from 1991 to 1994, where he had worked on Network Management. From 2009 to 2011, he served as the Director of the Institute of New Media and Communications. He is currently a Professor at SNU. He has been leading many industrial projects on 3G through 6G

and IoT connectivity supported by the Korean industry. He has published more than 300 technical articles and holds more than 100 patents. He received the KICS Haedong Scholar Award in 2012 and a national medal of honor for his contributions to education in 2025. He was President of the Korean Institute of Communications and Information Sciences (KICS). He served as Chief Information Officer (CIO) of SNU. He was General Chair of the IEEE WCNC 2020 (Wireless Communication and Networking Conference), IEEE ICCE 2020 (International Conference on Communications and Electronics), and IEEE DySPAN 2018 (Dynamic Spectrum Access and Networks). He was TPC Chair of the IEEE VTC-Spring 2014, and General Chair of JCCI 2015. He was Director of the Asia-Pacific Region of the IEEE ComSoc. He is an Editor of the IEEE Network Magazine, IEEE Transactions on Vehicular Technology, and IEEE Internet of Things Journal. He served as Co-Editor-in-Chief of the Journal of Communications and Networks (JCN), and was an editor of Computer Networks Journal and IEEE Tran. on Wireless Communications. He received a national medal of honor for his contributions to education and is a member of the National Academy of Engineering of Korea (NAEK).